Potential of environmental scanning electron microscopy and SAXS to determine structural insights of plant-based emulsions with increasing dry matter content

Theresia Heiden-Hecht[1,*], *Baohu* Wu[1], *Marie-Sousai* Appavou[1], *Stephan* Förster[2], *Henrich* Frielinghaus[1], and *Olaf* Holderer[1]

[1]Jülich Centre for Neutron Science (JCNS) at Heinz Maier-Leibnitz Zentrum (MLZ), Forschungszentrum Jülich GmbH, Garching, Germany

[2]Jülich Centre for Neutron Science (JCNS), Forschungszentrum Jülich GmbH, Jülich, Germany

Abstract.
Plant-based emulsions with increasing dry matter content show a large range of structural features from atomic to macroscopic length scales, which may be examined with scattering techniques in reciprocal space and microscopic techniques in real space. In this contribution, we focus on plan-based emulsions in terms of mesoscopic structure, and report on the impact of temperature and humidity on the structure measured via environmental scanning electron microscopy (ESEM) in real space. Small angle x-ray scattering in reciprocal space extends the knowledge on structural properties on smaller length scales at different temperature. Decreasing the humidity for the ESEM experiments revealed structural properties of different products. Temperature decrease from room temperature to 5 °C showed emerging crystalline peaks during SAXS measurements.

1 Introduction

Plant-based emulsions have a huge potential in substituting classical milk products [1]. A lot of research focuses on the implementation of novel plant proteins, and investigates the potential usage in plant-based emulsions with increasing dry matter content like milk drinks, fermented or heat-induced yoghurt or cheese like products [2, 3].

Imitating the texture and structure of dairy products is a challenge [4]. The texture and structure of emulsion products with different dry matter content is often analyzed via rheology, tribology and microscopy. Common microscopy methods in use are: transmission electron microscopy [5] and scanning electron microscopy [6, 7], both methods are used for studying casein micelles, confocal laser scanning microscopy [8, 9]. However, most of these methods have the disadvantage that an invasive sample preparation (freezing, cutting, substitution of water, staining, dye labelling) is required. Environmental scanning electron microscopy (ESEM) offers possibilities to investigate a range of samples in high resolution without invasive sample preparation, for example in Ref. [10] for a model cheese system. Varying pressure, temperature and with this combination also the relative humidity opens new possibilities in studying the morphology of food products on length scales below 1 μm to 1 mm. With small angle x-ray scattering (SAXS), complementary information in reciprocal space are accessible from the μm range down to atomic length scales (of the order of 0.1 nm)[11]. Also here, a rather natural environment with control parameters such as temperature are accessible.

This contribution shows some examples of how real space information obtained with environmental scanning electron microscopy (ESEM), complemented by reciprocal space information from small angle x-ray scattering (SAXS), can provide insight into plant-based emulsions and food products with different dry matter. Series of images with decreasing humidity in ESEM and scattering curves at two relevant temperatures are presented and discussed. The last section shows perspectives of neutron scattering to extend the range of scattering techniques for the characterization of food products [12]. Neutron scattering provides a view into these systems with different contrast and hence can reveal new structural details.

2 Methods

2.1 Environmental Scanning Electron Microscopy

The environmental scanning electron microscope (ESEM) provides the possibility to investigate surfaces with an electron beam without further treatment or coating, i.e. with almost no additional sample preparation, also for water containing samples, since a partial pressure of up to $\sim$ 800 Pa can be tolerated, corresponding to 100% relative humidity (r.h) at temperatures of 1.5-5°C. Reducing the pressure results in water evaporation revealing surface structural information of the non-water components [13, 14].

ESEM images were obtained at JCNS MLZ using a Thermo Fischer Quattro S ESEM (Thermo Fischer Sci-

*e-mail: t.heiden-hecht@fz-juelich.de

entific, Eindhoven, Netherlands) equipped with a 500μm aperture gaseous secondary electron detector (GSED). During observation, the temperature of the sample stage was controlled with a Peltier cooling system. All observations were carried out at a constant temperature of 2-5°C of the sample stage and the temperature of the samples was equilibrated for 15 min prior to any measurement. The relative humidity was controlled by changing the water vapor pressure in the chamber. The relative humidity (r.h.) is then 100% at a pressure of 800 Pa, shown as initial picture of all series. Subsequently, the pressure is lowered in two steps, to 350 Pa, corresponding to a r.h. of 50%, further to 105 Pa (r.h. 15%) and reversed to a r.h. of about 100%.

All ESEM experiments were carried out with the following operating conditions: 10 kV beam accelerating voltage for the samples PD1 "Drink1", PD2 "Drink1", PCC and PC, 5 kV was used for sample PY to diminish beam damage, spot size 3.0, sample working distance 6.7 +/- 1.2 mm, and and 5–10 us dwell time. The corresponding sample currents (measured in the Faraday cup in high vacuum) were 80 pA and 110 pA for 5 and 10 kV respectively. Secondary electron images were acquired via the integrated imaging software (xT microscope control) at 500, 650, 1000, and 1200 magnifications.

2.2 Small angle x-ray scattering

SAXS experiments were performed by a laboratory based SAXS beamline KWS-X (XENOCS XUESS 3.0 XL) at JCNS MLZ. The X-ray source is a D2+ MetalJet (Excillum) with a liquid metal anode operating at 70 kV and 3.57 mA with Ga-Kα radiation (wavelength λ = 1.314 Å). Samples were measured in a glass capillary at ambient pressure (1.5 mm ID) that was kept at 25°C or 5°C in a temperature controlled peltier stage. The sample to detector distances from 0.1 m to 1.70 m which cover the scattering vector Q range from 0.003 to 4 Å^{-1} (Q is the scattering vector, Q=$(4\pi/\lambda)sin(\Theta)$, 2Θ is the scattering angle). The SAXS patterns were normalized to an absolute scale and azimuthally averaged to obtain the intensity profiles, and the solvent background was subtracted.

2.3 Samples

We present results on two plant-based emulsions and three plant-based products with different amounts of dry matter, a yoghurt, a cream cheese and a cheese (all plant-based). Details of the samples are provided in Ref. [15], where plant-based and dairy emulsions and fermented emulsions are compared with respect to their structural characteristics. Here only the plant-based products are in the focus of interest. Table 1 lists the names and basic state of the sample.

Short name	Sample name Ref. [15]	State
PD1	Drink 1	Plant Drink 1
PD2	Drink 2	Plant Drink 2
PY	Ferm. 1-Y	Plant Yoghurt
PCC	Ferm. 3-CC	Plant Cream Cheese
PC	Ferm. 2-C	Plant Cheese

Table 1. Samples studied with ESEM and SAXS with short names. More details on the composition of the samples can be found in Ref. [15].

3 Results and Discussion

3.1 SAXS and ESEM

Plant-based emulsions and gelated emulsions were analyzed with ESEM and SAXS, the latter with a broad Q-range up to 4 Å^{-1}.

Surface structures on micrometer length scales were observed via ESEM by decreasing the r.h. from 100% down to 50%, 15% and then back to 100%. This series of images has been taken for two emulsions (PD1 and PD2), and three types of plant-based food products (PCC, creamy; PC, cheese like and PY, youghurt like). The series of pictures are presented in Figures 1 and 2 for the liquid emulsions and Figures 3, 4, and 5 for the plant-based food products with higher amounts of dry matter. For the latter two, all steps of the r.h. series are shown, for the first three only the 100% and 15% r.h. steps.

The two types of emulsions, PD1 and PD2, showed initially a smooth surface (as expected for a liquid), with reduced humidity a surface structure became visible, best at the lowest r.h. of 15% (Figures 1, 2). This process is reversible, an increase of r.h. leads to a fully smooth surface again. The emerging surface structures are in our point of view due to evaporation of water, and opposing water capillary effects exposing the structuring phase at the surface. The mobility of the low dry matter samples probably increases just enough to smoothen the surface again at high r.h., it is therefore not considered a macroscopic phase separation due to the soft environmental changes and conditions. Due to the relatively high hydrophobicity of the system, reducing the r.h. from 100 % to 15 % does not expel the hydration shell at the interfaces and is probably the reason for a certain reversibility upon rehydration as well as the high amount of water in the sample itself. The emerging structures of PD1 at low r.h. could be salts (Potassium phosphate and sea salts present in the solution) and fat droplets. A particle size analysis of 77 particles of the 15% r.h. sample showed a mean diameter of 6 μm (with a standard deviation of 3 μm). For PD2, structuring particle like elements seem to emerge at the top part of the image with diameters of about 8 μm and a rather broad distribution, difficult to assess because partly hidden in the interface. The time constant for recovery when going back to 100 % r.h. was about 5 min for PD1 and quasi-instantaneous for PD2.

The plant-based yoghurt (PY, yoghurt like) with low dry matter (Figure 3) showed a similar low structuring at the beginning at 100% r.h., which increased slightly upon drying at 50% r.h. with no further change when reducing the r.h. to 15%. Again, this process is reversible, increasing the r.h. to 100% leads again to a completely smooth surface. The associated length scales are of the order of some 10-50 μm similar to a fractal surface.

Other in the case of the second low dry matter cream cheese like product (PCC, Figure 4), where the structure consisting mainly of globular particles of very regular size

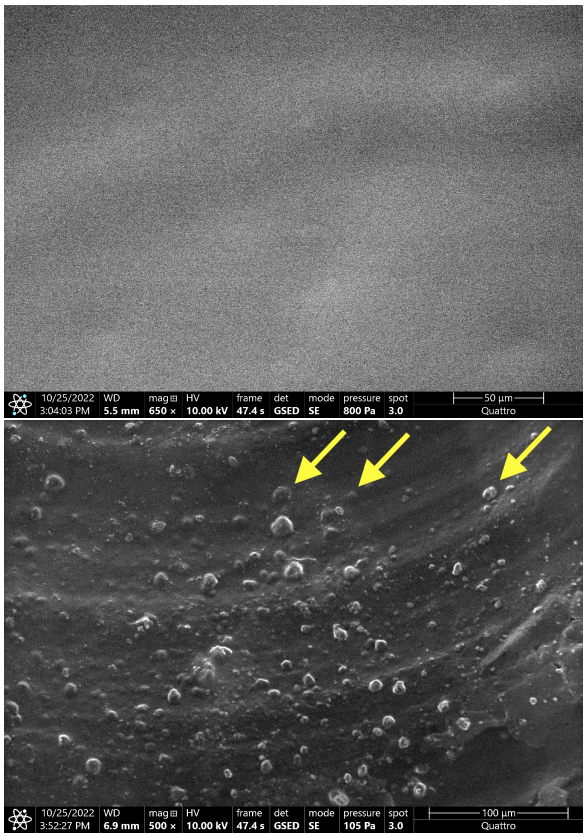

Figure 1. ESEM pictures at different relative humitidy of emulsion PD1, "Drink 1". From top to bottom, the r.h. was changed from 100% to 15%. Arrows mark some of the particles identified as most characteristic and discussed in the text.

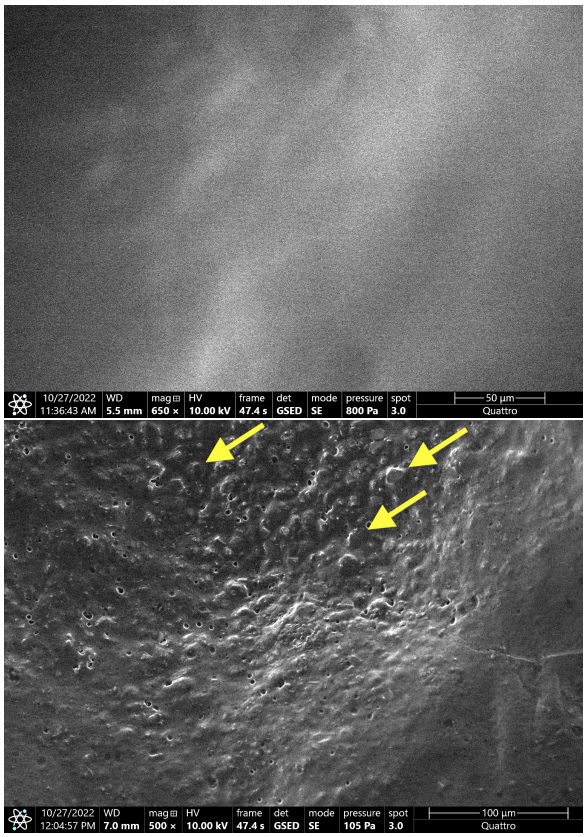

Figure 2. ESEM pictures at different relative humitidy of emulsion PD2, "Drink 2". From top to bottom, the r.h. was changed from 100% to 15%. Arrows mark some of the particles identified as most characteristic and discussed in the text.

of about 1.5 μm diameter (std dev. 0.3 μm, measured over 74 particles approximately at the same surface level in the image), which became visible upon reduction of humidity to 50% persisted also after re-hydration at the end of the experiment, probably due to the less mobile dry matter phase compared to the liquid drinks and the yoghurt like sample.

The high dry matter plant-based cheese PC 5 was much more solid and already well structured at 100% r.h. on the length scales of the ESEM experiment. It showed already at the initial 100% r.h. observation disperse globular structures of about 2-5 μm, and otherwise a rather fractal surface structure. There was no significant effect of changing the humidity.

With small angle x-ray scattering (SAXS) the three plant-based products PY, PCC and PC have been studied at two temperatures over a Q-range from 0.003-4 Å^{-1}, covering the typical small angle area with mainly a power law decay as well as the region where diffraction peaks from crystalline domains can be visible. The SAXS results of the two emulsions and the gels at room temperature have been discussed elsewhere [15] in more detail. Here the focus is on the temperature dependence of the three products. Figure 6 shows the full Q-range and a zoom into the high-Q-area of PY, PCC and PC at 25 °C and 5 °C. The power law decay is hardly affected by the temperature change, while on very small length scales a significant increase in crystallinity could be observed. The softest sample (top in Figure 6 is PY with low dry matter, as shown in the hydration change series in Figure 3, which stayed intact also when cooled down to 5 °C. PCC and PC showed an increase in crystalline features upon cooling. The Bragg peaks visible for the low (PCC) and high (PC) dry matter fermented emulsions (middle and bottom of Figure 6) at Q$\simeq 0.15 - 0.17$ Å^{-1} stem from aligned fat molecules from either coconut oil [16] for PC or from rapeseed oil for PCC (middle) [17] which is already present in a partly aligned form at 25 °C but which increases in ordering at 5 °C.

At higher Q above 1 Å^{-1} local ordering also increased with decreasing temperature significantly for PC, while for PCC it was already initially in a partly ordered state and only sharpened slightly.

The length scales covered by the SAXS experiments here, $d = 2\pi/Q$, are approximately 2 μm to 2 Å. The ESEM images shown here complement the length scale range towards larger structures. The slope of the SAXS intensities at low Q has been analyzed in Ref [15] with $I(Q) \propto Q^{-3.2}$ to $Q^{-3.9}$ indicating a surface fractal structure on these length scales below the length scales of the ESEM images, which seems quite consistent with the ESEM images at low relative humidity. While SAXS provides truly a view into the bulk structure, with the property that an ensemble average of the structures in the probed volume is represented in the scattering curves, the ESEM technique

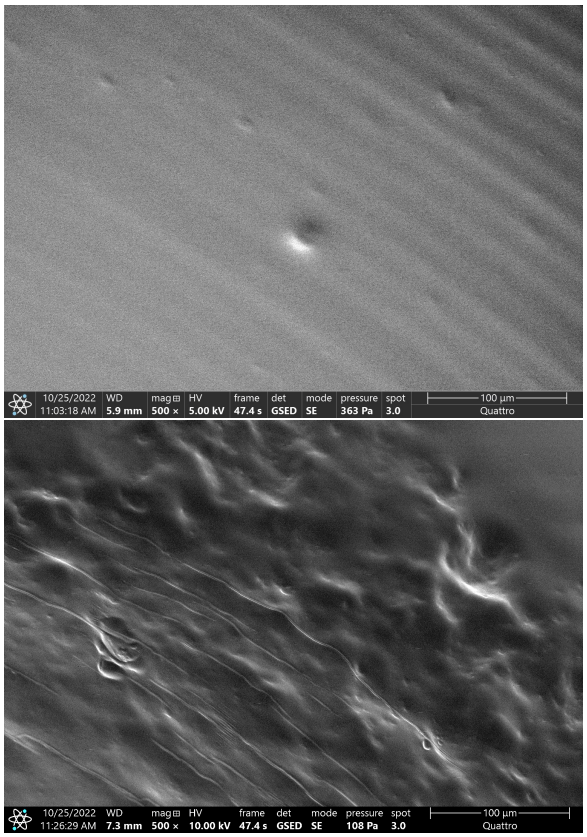

Figure 3. ESEM pictures of PY, a plant-based yoghurt with low dry matter, at r.h. of 100% (top) and 15% (bottom).

shows the surface morphology of a cut through the sample or of the liquid droplet surface, at different temperature/pressure conditions. From the images presented here it is also obvious that the 100% r.h. images often do not show any significant structuring in the cuts of the soft matter samples, but that contrast between parts with different vapor pressure may be created by reducing the relative humidity. It can therefore complement scattering information with respect to larger length scales and with insight into structuring elements emergent under vapor evaporation.

3.2 Outlook: neutron perspectives

The main advantage for neutron scattering in the area of food gels and emulsions is the possibility to investigate thick and nontransparent samples, with less radiation damage or heating as with x-rays due to the much lower kinetic energy of the neutron beam, and the possibility of varying the contrast by partially deuterating components of such multicomponent systems as the food emulsions. Small angle neutron scattering (SANS) provides a broad range of scattering vectors, and it can be extended towards low Q with double crystal diffractometers or with spin echo resolved SANS (SESANS)[18], or finally radiography for real space information, and to high Q with classical diffractometers. This also offers the possibility to access length scales from millimeters to Angstroem, but requires normally to generate model systems by partly deuterating the samples, in the simplest case only by ex-

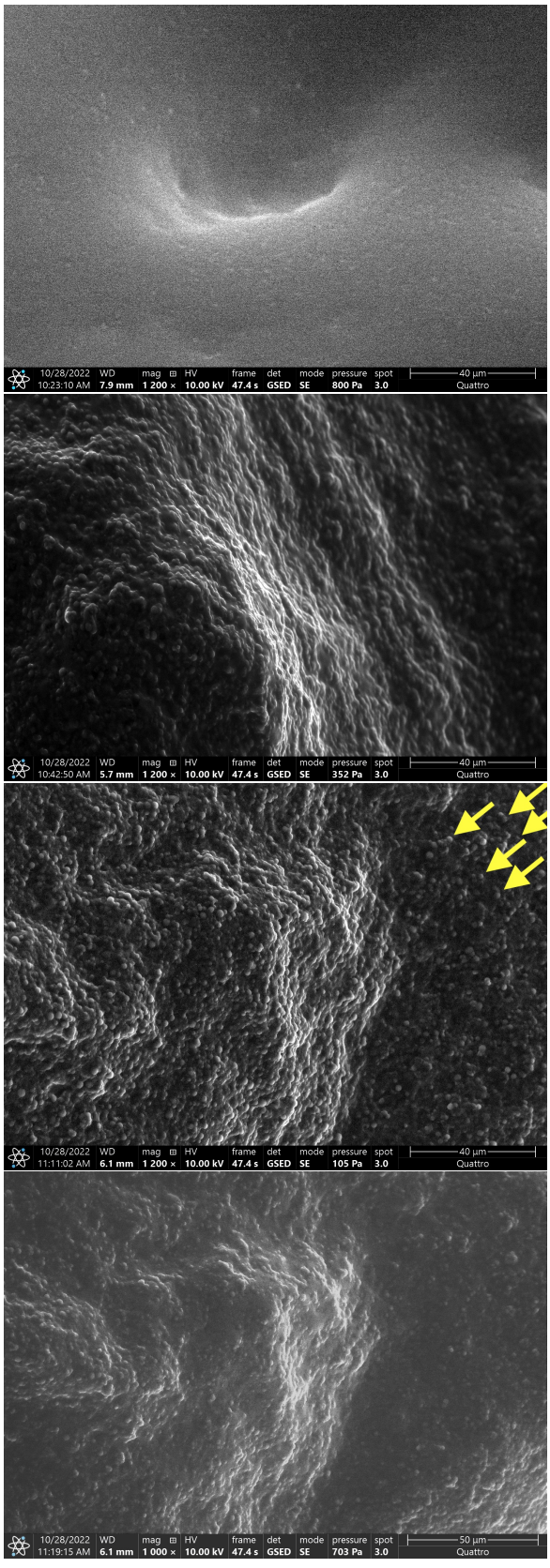

Figure 4. ESEM images of a plant-based cream cheese PCC with low dry matter at a r.h. of 100% to 50%, 15%, back to 100% (top to bottom). Arrows mark some of the particles identified as most characteristic and discussed in the text.

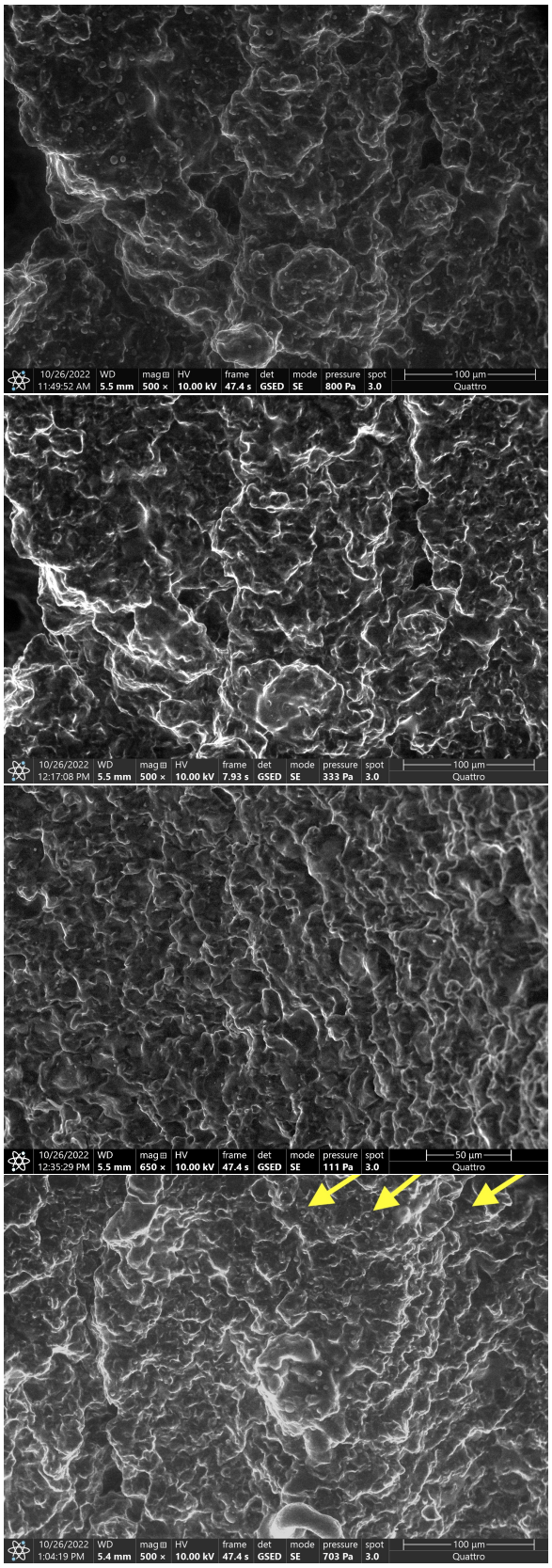

Figure 5. ESEM images of the plant cheese PC with high dry matter at a r.h. of 100% to 50%, 15%, back to 100% (top to bottom). Arrows mark some of the particles identified as most characteristic and discussed in the text.

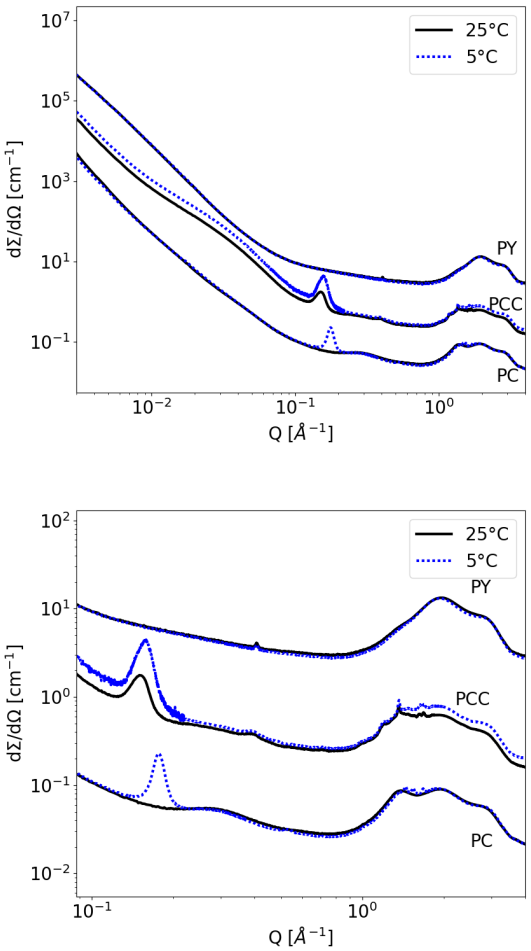

Figure 6. Top: Small Angle X-ray Scattering over a broad Q-range. From top to bottom PY, PCC, PC, measured at 25 °C and 5 °C. Bottom: zoom into the region of larger Q.

changing the water contents with heavy water, or by more advanced contrast variation methods, with deuterated oils, lipids or proteins, which would fully exploit the strength of neutron scattering. The results presented here were obtained on commercially available food products. Studying related model systems with selective deuteration and contrast variation allows to address specific questions with neutron scattering, such as details of the origin of different features from the SAXS results.

4 Conclusion

This contribution briefly illustrates how combining scattering techniques as an ensemble average in reciprocal space and microscopy such as ESEM as a high resolution technique without the need of extensive sample preparation and modification can lead to interesting information about structural features on length scales relevant for the texture, for the rheological and stability properties of gels made from plant-based food emulsions. ESEM provides the possibility to observe humid samples and to vary humidity in the sample chamber and hence observe surface structures during de-hydration and re-hydration in situ, but is mainly

restricted to observations of the surface or cuts through the bulk. SAXS is a complementary technique in reciprocal space, able to observe ensemble averaged structural features from sub-nm to micrometer length scales. Crystallisation of fat molecules on length scales of nanometers as well as crystal structures possibly from salt crystals on sub-nanometer length scales could be observed. A power law decay from the larger scale structures can be observed. More details are expected from further neutron scattering studies, where the contrast between different domains and areas in the sample can be modified by using partly deuterated compounds such as deuterated water, oil, proteins or lipids. This requires to prepare comparable samples to the consumer products shown here in a controlled manner in the lab. Linking the information on this important range of length scales with macroscopic rheological properties might be the path of systematically improving food based fermented emulsions such as plant-based cheese or yoghurt. Since the study of plant-based emulsions and gels is only at its very beginning, we think that these techniques might contribute in the future significantly to further investigate and develop new products in this emerging sector.

Data availability statement

The data from the SAXS and ESEM experiments are available from the corresponding author upon reasonable request.

Acknowledgement

This work is based upon experiments performed at the ESEM and KWS-X instrument operated by Forschungszentrum Jülich at the Heinz Maier-Leibnitz Zentrum (MLZ), Garching, Germany. The Thermo Fischer Quattro S ESEM is located at the Meier-Leibnitz Zentrum in Garching and is jointly operated by Helmholtz-Zentrum Hereon and Forschungszentrum Jülich.

References

[1] W. Kim, Y. Wang, C. Selomulya, Trends in Food Science Technology **105**, 261 (2020)

[2] M. Brückner-Gühmann, E. Vasil'eva, A. Culetu, D. Duta, N. Sozer, S. Drusch, Journal of the Science of Food and Agriculture **99**, 5852 (2019)

[3] M. Brückner-Gühmann, A. Kratzsch, N. Sozer, S. Drusch, Future Foods **4**, 100053 (2021)

[4] P. Fischer, E.J. Windhab, Current Opinion in Colloid Interface Science **16**, 36 (2011)

[5] T. Kamigaki, Y. Ito, Y. Nishino, A. Miyazawa, Microscopy **67**, 164 (2018)

[6] J. Glaser, P.A. Carroad, W.L. Dunkley, Journal of Dairy Science **63**, 37 (1980)

[7] D.J. McMahon, W.R. McManus, Journal of Dairy Science **81**, 2985 (1998)

[8] J. Blonk, H. Van Aalst, Food research international **26**, 297 (1993)

[9] M. Ferrando, W. Spiess, Food Science and Technology International **6**, 267 (2000)

[10] N. Castaneda, Y. Lee, Gels **5** (2019)

[11] E.P. Gilbert, Current Opinion in Colloid and Interface Science **42**, 55 (2019)

[12] A. Lopez-Rubio, E.P. Gilbert, Trends in Food Science and Technology **20**, 576 (2009)

[13] A. Donald, Nature materials **2**, 511 (2003)

[14] D.J. Stokes, Microscopy and Analysis **26(6)**, 67 (2012)

[15] T. Heiden-Hecht, B. Wu, M.S. Appavou, S. Förster, H. Frielinghaus, O. Holderer, submitted (2023)

[16] X. Meng, Q. Pan, Y. Ding, L. Jiang, Food chemistry **147**, 272 (2014)

[17] Y. Miyagawa, K. Shintani, K. Katsuki, K. Nakagawa, S. Adachi, Food Structure **11**, 8 (2017)

[18] W.G. Bouwman, Food Structure **30** (2021)